Journal of Biomolecular NMR, **17:** 17–32, 2000.
KLUWER/ESCOM

Accuracy of bound peptide structures determined by exchange transferred nuclear Overhauser data: A simulation study

Elan Zohar Eisenmesser[a,*], Adam P.R. Zabell[b,*] & Carol Beth Post[b,**]
[a]*Department of Biological Sciences, Purdue University, West Lafayette, IN 47907-1392, U.S.A.;* [b]*Department of Medicinal Chemistry, Purdue University, West Lafayette, IN 47907-1333, U.S.A.*

Received 30 September 1999; Accepted 7 March 2000

Key words: exchange-transferred NOESY, NMR computer simulation, NMR structure, NOE rate-matrix analysis

Abstract

The exchange-transferred NOE method to determine the three-dimensional structure of peptides bound to proteins, or other macromolecular systems, is becoming increasingly important in drug design efforts and for large or multicomponent assemblies, such as membrane receptors, where structural analysis of the full system is intractable. The exchange-transferred nuclear Overhauser effect spectroscopy (etNOESY) method allows the determination of the bound-state conformation of the peptide from the intra-molecular NOE interactions between ligand protons. Because only ligand–ligand NOEs are generally observable, the etNOESY method is restricted to fewer NOEs per residue than direct protein structure determination. In addition, the averaging of relaxation rates between free and bound states affects the measured cross-peak intensities, and possibly the accuracy of distance estimates. Accordingly, the study reported here was conducted to examine the conditions required to define a reliable structure. The program CORONA was used to simulate etNOE data using a rate-matrix including magnetic relaxation and exchange rates for two peptide–protein complexes derived from the reference complex of cAMP-dependent protein kinase ligated with a 24-residue inhibitor peptide. The results indicate that reasonably accurate peptide structures can be determined with relatively few NOE interactions when the interactions occur between non-neighboring residues. The reliability of the structural result is suggested from the pattern of NOE interactions. A structure with an accuracy of approximately 1.3 Å rms difference for the main-chain atoms can be obtained when etNOE interactions between non-neighboring residues occur over the length of the peptide. The global precision is higher (approximately 0.9 Å rms difference) but is not correlated to global accuracy. A local definition of precision along the backbone appears to be a good indicator of the local accuracy.

Abbreviations: etNOE, exchange transferred nuclear Overhauser effect; PKA, cAMP-dependent protein kinase; PKI, inhibitor peptide of PKA; CORONA, program for calculated or observed NOESY analysis; rMD, restrained molecular dynamics.

Introduction

The methodology using exchange-transferred nuclear Overhauser spectroscopy (etNOESY) to determine the three-dimensional structure of a small molecule ligand when bound to a protein is becoming increasingly important in drug design efforts and for large protein assemblies where structural analysis of the full system is found intractable (Ni and Scheraga, 1994; Fraenkel et al., 1996). The method may be applied under variable solution conditions where appropriate binding exists (Clore and Gronenborn, 1983; Campbell and Sykes, 1993; Ni, 1994). This ability to obtain three-dimensional structural information about a ligand is a valuable complementary approach, both to crystallography in the absence of crystals and to the direct NMR method for very large molecular-

*Both of these authors contributed equally to this work.
**To whom correspondence should be addressed. E-mail: cbp@cc.purdue.edu

weight systems. Exchange-transferred NOESY was first used for three-dimensional structural determination with nicotinamide-adenine dinucleotide (Albrand et al., 1979; Clore and Gronenborn, 1983; Feeney et al., 1983; Levy et al., 1983; Andersen et al., 1985; Machida et al., 1985), and has since been applied to flexible peptides (Scherf et al., 1992; Matsunaga et al., 1993; Andrieux et al., 1995; Schneider and Post, 1995; Mayo et al., 1996; Burritt et al., 1998; Eisenmesser and Post, 1998; Fraternali et al., 1998; Gizachew et al., 1998; Kobayashi et al., 1999). When the ligand has few degrees of freedom, a small number of distance estimates can readily resolve possible conformations, while the determination of the bound structure of larger, more flexible ligands using the etNOESY method is more challenging. Only ligand–ligand NOE interactions are readily measured by the etNOESY experiment.[1] Because the density of tertiary interactions is lower for a peptide than for a globular protein, there are fewer NOE interactions, and hence distance restraints, per residue for a peptide. In addition, a small-molecule peptide ligand lacks the extensive packing interactions of folded proteins, and thus the advantage close packing confers by limiting the number of energetically favorable conformations. Structural characterization of a peptide ligand by etNOE differs even from that of a protein surface loop which is covalently constrained at one or both ends and usually shows NOE interactions by packing with other parts of the protein. These factors present the need for assessing the accuracy of etNOE structures. Accordingly, we undertook this study to examine the etNOESY requirements which define a reliable structure.

We report a simulation study to examine the accuracy of bound peptide structures determined from etNOESY data using distance-restrained molecular dynamics (rMD). The crystallographic structure of cAMP-dependent protein kinase (PKA) bound with the peptide inhibitor PKI(5–24) (Knighton et al., 1991) was used to simulate etNOESY data from a full rate matrix analysis with the program CORONA (Zheng and Post, 1993, 1996). Two 13-residue regions from PKI were modeled in order to examine different structure types. Effects of exchange on the interpretation of ligand interproton distances from the etNOE intensity were considered. Various protocols and force fields were used with rMD coupled to high-temperature annealing (Clore et al., 1986, 1987; Metzler et al., 1989), or with increased dimensionality to four spatial dimensions (van Schaik et al., 1993). The results indicate that reasonably accurate peptide structures can be determined with relatively few NOE interactions when the interactions occur between non-neighboring residues. The reliability of the structural result is suggested from the pattern of NOE interactions. In addition, local precision of the set of NMR structures appears to be a good indicator for deciphering accurate local structure.

[1] Although some ligand–protein interactions have been measured (Ramesh et al., 1996; Casset et al., 1997; Poppe et al., 1997; Sokolowski et al., 1998), these are too few to be considered generally useful for structure determination.

Methods

Reference structures

Two reference complexes were constructed from the energy-minimized ternary complex PKA•ATP•PKI(5–24) (PDB accession code 1ATP) differing only in the residues selected from PKI(5–24). The peptide ligand, 13 residues in both complexes, begins either at residue 5, PKI(5–17), TTYADFIASGRTG-NH_2, or at residue 9, PKI(9–21), acet-DFIASGRTGRRNA-NH_2. The numbering of the peptide residues comes from the inhibitor protein from which it is derived (Walsh et al., 1971; Ashby and Walsh, 1972). Protons were built onto the heavy-atom positions using the HBUILD command in CHARMM (Brooks et al., 1983). Crystallographic coordinates within 20 Å of PKI(5–24) were subjected to 700 steps of conjugate gradient energy minimization (Fletcher and Reeves, 1964). The rms difference of the main-chain atoms of the peptide before and after energy minimization was 0.53 Å.

etNOESY simulations

Coordinates of the two peptide–protein complexes were used to calculate etNOESY cross-peak intensities with the rate-matrix program CORONA (Calculated OR Observed NOESY Analysis). CORONA provides the full matrix solution to the simultaneous Bloch equations for cross relaxation in proteins or nucleic acids, given either a structure or a set of NOE intensities from one- or two-dimensional data (Post et al., 1990). In addition to the spin-diffusion effects accounted for by the rate matrix analysis, the effects of exchange were included in the simulation of etNOESY intensities with CORONA (Zheng and Post, 1993, 1996). Methyl group rotations were explicitly taken into account, but no other internal motions in

the bound peptide were considered. The exclusion of internal motion in this initial simulation study of the exchange-transferred NOE method for structure determination is reasonable given that the error introduced by assuming a rigid molecule instead of one with internal, thermal motion has been shown to be small when applying approximate distance restraints (Post, 1992). Protons on the peptide and any protein proton within 8.0 Å of any peptide atom, excluding exchanging hydrogens from Ser, Thr, and Tyr side chains, were included in the matrix analysis. The correlation times for the free ligand (τ_{lig}) and the complex (τ_{cmplx}) were estimated from molecular weight to be 0.64 ns and 18.3 ns, respectively. A PKA concentration of 0.5 mM and peptide concentration of 5.0 mM were assumed. A dissociation constant of 100 μM places the system in the fast-exchange limit, and gives 98% of the enzyme in the bound state. A mixing time of 100 ms and a spectrometer frequency of 500 MHz were used.

Distance restraints

Two distance-restraint lists were generated in this study. To simulate a practical approach for estimating distance restraints, the first list was obtained by categorizing the etNOE volumes into strong, medium and weak interactions. This SMW list corresponds to lower and upper bounds in the square well potential of 1.8–2.7 Å, 1.8–3.3 Å and 1.8–5.0 Å, respectively. The volume intensity between the Hδ and Hε ring protons of Phe 10 was used as an internal reference for categorizing the restraints in both SMW lists since this aromatic residue is common to both peptide models. This reference is the average intensity for two NOE pairs ($H_{\delta 1}$-$H_{\varepsilon 1}$ and $H_{\delta 2}$-$H_{\varepsilon 2}$), each with a fixed interproton distance of 2.45 Å. The intensities of the Hδ–Hε peaks were not significantly altered by relaxation from Hη. The remaining NOE intensities were categorized as strong, medium, or weak, assuming an r^{-6} dependence of the cross-peak intensity. Intensities less than 5% of the reference intensity were considered to fall below a baseline noise level and excluded. This procedure generated a total of 141 restraints for PKI(5–17) and 145 for PKI(9–21). A second restraint list, with the same proton pairs as the SMW list, was generated in order to assess the influence of error in the distance estimates on the structural accuracy. This EXACT list of distance restraints used an upper bound equal to the actual distance in the reference structure and set the lower bound to 1.8 Å.

By their nature, etNOE experiments must handle a large number of degenerate chemical shifts since the observed, exchange-averaged chemical shift is dominated by the free peptide chemical shift. Thus, methylene and aromatic side-chain protons are often closely overlapped or magnetically equivalent due to motional averaging. Moreover, even in cases where methylene proton resonances are resolved, stereospecific assignments are rarely obtained. Accordingly, the etNOE intensities for all methyl and methylene protons, as well as the Tyr and Phe side-chain Hδ and Hε protons were treated as degenerate or overlapped peaks by summing the appropriate calculated intensities. The average intensity was categorized and the restraint applied to the entire set of degenerate protons (e.g. HB*–HG*). Each CHARMM rMD test method (see below) used a simple distance averaging for degenerate protons (REXP = 1) while the XPLOR approach averaged r^{-6} values for degenerate protons (AVER ∗ R–6).

Structure determination approaches

The SMW and EXACT distance restraints generated from each of the two peptide complexes were used in rMD calculations of the isolated peptides with four approaches using CHARMM and one using X-PLOR 3.1 (Brünger, 1992), as outlined in Table 1. All CHARMM calculations employed the CHARMM22 parameters, files top_allh22_prot.inp and par_allh22_prot.inp (MacKerell et al., 1998), modified as previously described (Eisenmesser and Post, 1998) to ensure tyrosine and phenylalanine ring planarity, and to maintain a trans peptide bond during high temperature simulations. A square well potential was used for the distance restraints with k_{noe} equal to 50 kcal mol^{-1} Å^{-2}. The X-PLOR parameters were defined by topallhdg.pro and parallhdg.pro with a soft square-well potential for the distance restraints, k_{noe} equal to 50 kcal mol^{-1} Å^{-2}, and a linear slope equal to 1.0 (Kraulis et al., 1989; Brünger, 1992).

The four different CHARMM approaches varied the force field and the molecular dynamics algorithm. The first two employed the CHARMM22 force field, either with or without electrostatics, and are referred to as C1 and C2, respectively. The second two CHARMM approaches implemented molecular dynamics in four spatial dimensions (4D) for the Lennard-Jones potential and excluded electrostatics. A harmonic potential imparted on the fourth dimensional coordinate controlled the extent to which the system moved in 4D space (van Schaik et al., 1993). The first of these two 4D approaches, C3, used an initial rMD temperature of 300 K, and a fourth dimen-

Table 1. rMD approaches used in this study

Approach	Parameters	Electrostatics	Steric restraint	Dimensionality	Initial SA temp
C1	CHARMM	Y	vdW	3D	1000
C2	CHARMM	N	vdW	3D	1000
C3	CHARMM	N	vdW	4D	300
C4	CHARMM	N	vdW	4D	1000
X1	X-PLOR	N	repel	3D	1000
UNRSTR	CHARMM	Y	vdW	3D	1000

sional force constant, k_{4D}, of 0.239 kcal mol^{-1} Å^{-2}. During cooling, the system was brought to 0 K for the fourth dimension while k_{4D} was increased stepwise to 23.9 kcal mol^{-1} Å^{-2}. The second 4D approach, C4, brought the initial rMD temperature to 1000 K and set k_{4D} to 2.39 kcal mol^{-1} Å^{-2}. Again, the 15 ps of cooling brought the fourth dimension to 0 K with a stepwise linear increase in k_{4D} to 239.0 kcal mol^{-1} Å^{-2}.

The fifth approach, X1, employed the X-PLOR program and its force field developed to efficiently search conformational space at high temperatures. No electrostatics are included, and a simple repulsive term replaces the van der Waals expression.

Lastly, a set of 10 structures for PKI(5–17) and PKI(9–21), five beginning from the minimized α-helix and five beginning from the minimized extended strand of each peptide sequence, were generated using no restraints and the C1 test case. These structures are referred to as the UNRSTR approach.

Each approach used the following rMD protocol except as noted above for C3 and C4. Fifty structures starting from a right-handed α-helix and fifty structures starting from an extended chain were generated, beginning with different random seeds for initial velocities. Both starting structures had been subjected to energy minimization prior to molecular dynamics. The Verlet algorithm (Verlet, 1967), and a 1 fs timestep were used for 30 ps of rMD at 1000 K followed by cooling to 100 K over a 15 ps period. Structures calculated from the different rMD approaches were then subjected to 3500 steps of restrained conjugate gradient minimization in CHARMM using a full Lennard-Jones potential and electrostatics with a distance dependent dielectric and k_{noe} equal to 50 kcal mol^{-1} Å^{-2}. This final optimization of all structures against the same force field was essential for a meaningful comparison of the final structures.

From each set of 100 structures produced with each approach, 10 structures were selected based on low NOE energy and acceptable ϕ, ψ values (Gunasekaran et al., 1996; Kleywegt and Jones, 1996). The average structure for each subset was calculated after a least squares superposition of all heavy atoms, and then optimized by 3500 steps of energy minimization with k_{noe} equal to 50 kcal mol^{-1} Å^{-2}.

Results and discussion

In the PKA–PKI complex (Knighton et al., 1991), PKI binds in a conformation which has both a helical (residues 5 to 13) and an extended region (residues 14 to 24). Two 13-residue reference complexes were derived from the crystallographic complex in order to evaluate structure determination for a case where the peptide ligand is a recognizable helix – PKI(5–17) – and a case where the peptide ligand lacks any significant secondary structure – PKI(9–21).

Exchange-transferred NOE intensities

Exchange-transferred NOESY intensities were calculated with the program CORONA (Zheng and Post, 1993) using a rate matrix comprising magnetic relaxation and exchange rates for all peptide protons and protein protons which lie within 8.0 Å of the peptide. The *n* peptide protons and *m* protein protons give rise to a $(n + m) \times (n + m)$ symmetric matrix that includes rates corresponding to both free and bound states of peptide and protein. The calculated intensities therefore include contributions from spin diffusion through both intramolecular and intermolecular dipolar interactions, as well as the relaxation effects due to the exchange process. For PKI, *n* equals 92 or 111 protons, while *m* equals 192 and 332 protein protons for the complexes with PKI(5–17) and PKI(9–21), respectively. The extended structure of PKI(9–21) leads

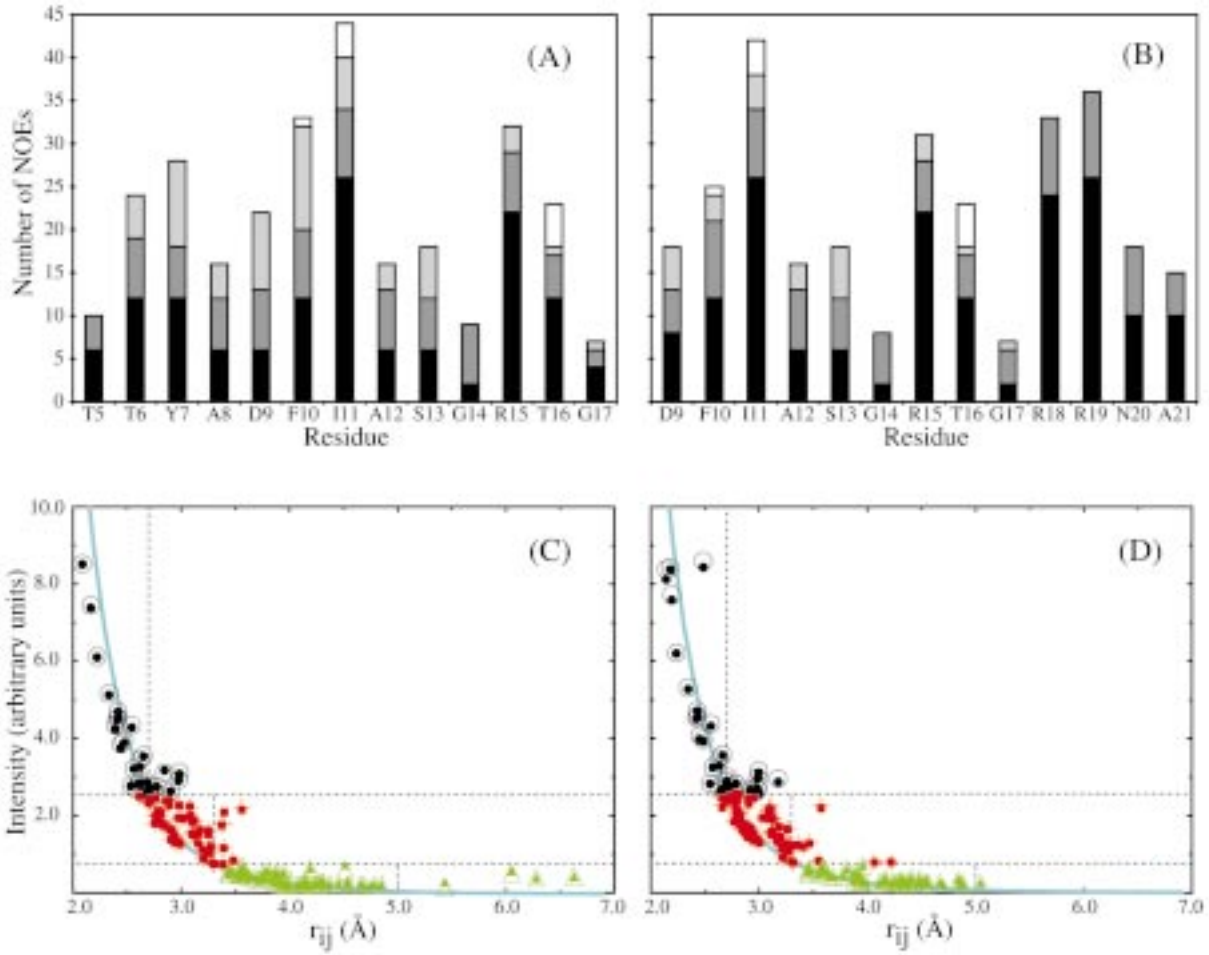

Figure 1. (A) Number of NOEs per residue for PKI(5–17) broken down by type of NOE pair to intraresidue (black), sequential (dark gray), short range ($2 \leq |i - j| \leq 5$, light gray) and long-range ($|i - j| > 5$, white). Each member of the NOE pair is counted separately, consequently the numeric total displayed is twice the number of NOEs used in the simulations. (B) Same as (A) but for peptide PKI(9–21). (C) CORONA determined peak intensity versus known crystallographic distance for strong (solid black circles), medium (solid red squares), and weak (solid green triangles) restraints for PKI(5–17) assuming fully protonated PKA. The same calculations were performed assuming a fully deuterated PKA, again breaking down the restraints to strong (open circles), medium (pluses), and weak (open triangles) restraints. Horizontal lines correspond to the intensity cutoff between restraint classification and vertical lines correspond to the expected distance cutoff for each classification. Distances for degenerate protons (see text) were calculated as the linear average. (D) Same as (C) but for peptide PKI(9–21).

to the larger number of protein protons in the matrix calculations.

The distribution by residue of etNOE intensities is shown in Figure 1A and 1B for PKI(5–17) and PKI(9–21), respectively. The number of distance restraints estimated from these intensities is 141 for PKI(5–17) and 145 for PKI(9–21). While the total number per peptide is similar, the number of intraresidue and interresidue restraints differs. Specifically, residues 18 to 21 in PKI(9–21) are in an extended conformation and have no medium ($2 \leq |i - j| < 5$) or long-range ($|i - j| \geq 5$) NOE interactions, while all but residues 5 and 14 in PKI(5–17) have at least medium-range interactions.

Accuracy of SMW *distance restraints*

Calculation of the etNOE intensities and estimation of interproton distances based on these intensities allows an evaluation of the reliability of categorizing distances based on strong, medium and weak etNOE intensity. The accuracy of distance estimates was discussed in simulation studies of direct NOE measurements (Post et al., 1990; Hoogstraten and Markley, 1996). This work builds upon these earlier studies by considering aspects specific to exchange systems. The

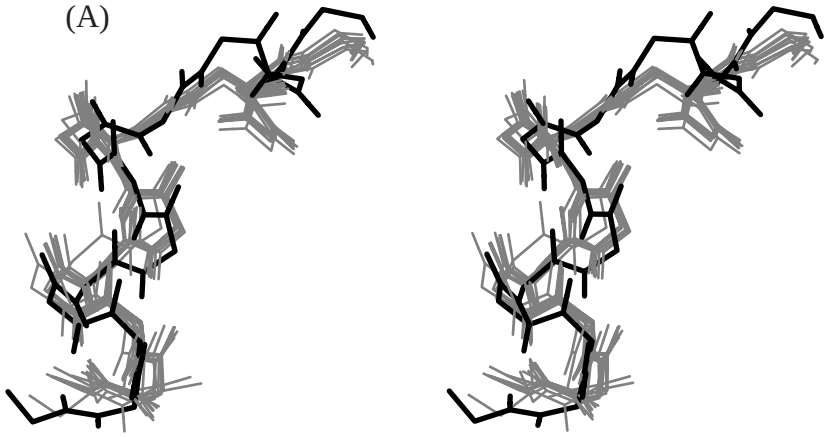

Figure 2. (A) Stereoview of a main-chain superposition of the best 10 structures of PKI(5–17) from the C2 SMW restraints. The reference structure for this segment of PKI is shown in bold. (B) Same as (A) but with PKI(9–21). (C) Same as (B) but with a superposition of MC_{sel}, main-chain atoms for residues 9–17.

averaging of relaxation rates in an exchange system, and the high molecular weight of the protein complex (typically >75 kDa) affect the manner in which magnetization diffuses through the system, and potentially propagates into errors in distance estimates.

The reliability of evaluating distance restraints based on SMW intensity categories is illustrated in Figure 1C and 1D for PKI(5–17) and PKI(9–21), respectively, by plotting the intensity as a function of the actual distance in the known complex. The intensity threshold separating strong (solid black circles), medium (solid red squares) or weak (solid green triangles) intensities is indicated by horizontal lines, with the upper limit of the restraint function marked by a vertical line for each category. The lower limit is approximated by a van der Waals contact of 1.8 Å for all categories and not shown. Examination of Figure 1C and 1D finds that the large majority of distance restraints are properly categorized based on SMW intensities. A small number of intensities (<10%) lie to the right of the vertical line of each category, and result in incorrectly categorized distance restraints when using linear averaging. The error associated with most of these interactions is small (<0.5 Å), except for four long-distance interactions in PKI(5–17) (Figure 1C). Transferred NOESY intensities may deviate from the ideal r^{-6} dependence for several reasons. In addition to the intramolecular spin diffusion common to all cross-relaxation in macromolecules, deviations specific to exchange systems can arise from intermolecular spin diffusion, free peptide relaxation, or the presence of degenerate or non-stereospecifically assigned resonances.[2] The sources of error in categorizing restraints were found to be intra-molecular spin diffusion and averaging of degenerate resonances. Neither intermolecular spin diffusion nor free peptide relaxation contributed significantly. Effects from intramolecular spin diffusion have been well documented and are only mentioned here as one source of error in distance estimates. The remaining three issues are discussed below.

Intermolecular spin diffusion. The potential for indirect contributions from spin diffusion between the ligand and macromolecule to ligand–ligand cross peaks has been identified by several investigators (London et al., 1992; Zheng and Post, 1993; Ni and Zhu, 1994; Arepalli et al., 1995; Jackson et al., 1995; Moseley et al., 1995; Barsukov et al., 1996). The possible existence of intermolecular spin diffusion was tested here by simulating the etNOE intensities for fully deuterated PKA. These intensities, plotted in Figure 1C and 1D using open circles, crosses, or open triangles, differ insignificantly from the intensities calculated with protonated PKA. A comparison of ligand cross-peak intensities observed experimentally with protonated and perdeuterated protein also found negligible differences (Barsukov et al., 1996). The lack of an effect from intermolecular spin diffusion for PKI•PKA is due to the manner in which the peptide binds; PKI

[2]Degenerate or non-stereospecifically assigned resonances are a relatively more important consideration for etNOE since the observed frequency values correspond to free peptide; aromatic and most methylene resonances are not resolved. Stereospecific assignments are not made due to lack of J coupling data.

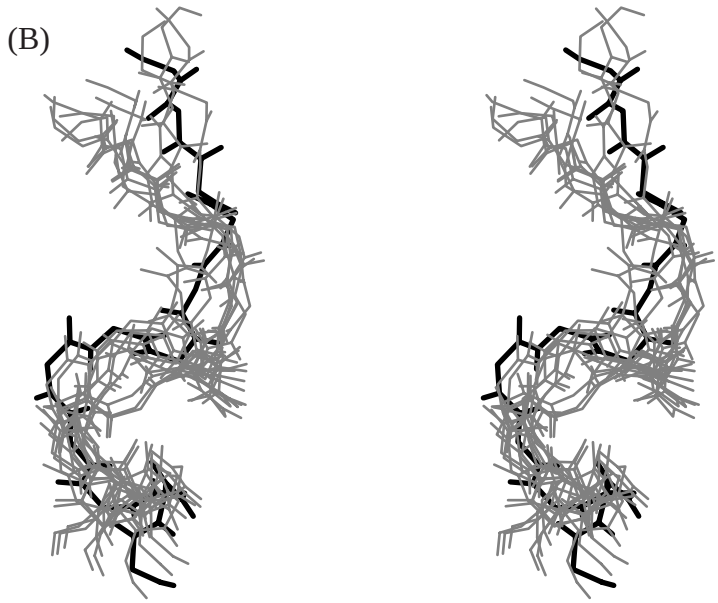

Figure 2. (continued).

binds primarily to the protein surface, with little opportunity for effective cross-relaxation via protein protons for any specific pair of ligand protons. Indeed, an examination of all peptide–peptide pairs with less than 4.0 Å separation found no protein proton within a short enough distance to have an Overhauser effect beyond that due to peptide relaxation pathways. The calculated intermolecular spin-diffusion effect from this spatial arrangement of spins becomes apparent only at long mixing times (at least 300 ms) and/or low ligand:protein ratios (results not shown). Earlier experimental studies, which showed that protein relaxation pathways contribute to particular ligand–ligand etNOE intensities (Zheng and Post, 1993; Arepalli et al., 1995; Vincent et al., 1997; Sokolowski et al., 1998), involved ligands that bind with some portion deeply buried within the protein, and are thus more likely to have nearby protein protons providing an efficient relaxation pathway.

Free peptide relaxation. When performing etNOE-based structure determinations, two types of relaxation from the free peptide can affect the observed etNOE intensity. Cross-relaxation in the free state, σ_f, would contribute to the observed NOE intensity according to the fractional molarity of unbound peptide when fast exchange conditions apply (Clore and Gronenborn, 1983). Nonetheless, σ_f is small in this simulation study, as is generally the case for flexible peptides with a short correlation time and random averaging of interproton distances. A second relaxation effect less commonly recognized is the loss of NOE intensity due to T_1^{free} (Campbell and Sykes, 1991; Zheng and Post, 1993). This effect increases at longer mixing times and higher free to bound peptide ratios, but under the conditions simulated in this study, it is not significant.[3]

Degenerate and non-stereospecifically assigned resonances. A third source of error in estimating distance restraints for etNOE is the problem of many degenerate cross peaks and lack of stereospecific assignments for the free peptide resonances. Numerous approaches exist to take into account multiple interproton distances in applying a single distance restraint. This work has utilized linear-distance averaging and r^{-6} averaging. These errors are approximately 0.5 Å, and are smaller for r^{-6} rather than linear averaging of degenerate pairs.

NMR structure determination

NMR structures were generated in vacuo by restrained molecular dynamics using different force fields and protocols for the five approaches outlined in Table 1. Either SMW or EXACT restraint lists were applied to

[3]The insignificance of σ_f or T_1^{free} can be easily validated experimentally by measuring the NOE intensity of free peptide under the conditions of the etNOE experiment, or by varying the protein/peptide ratio and measuring the change in σ_{obs}.

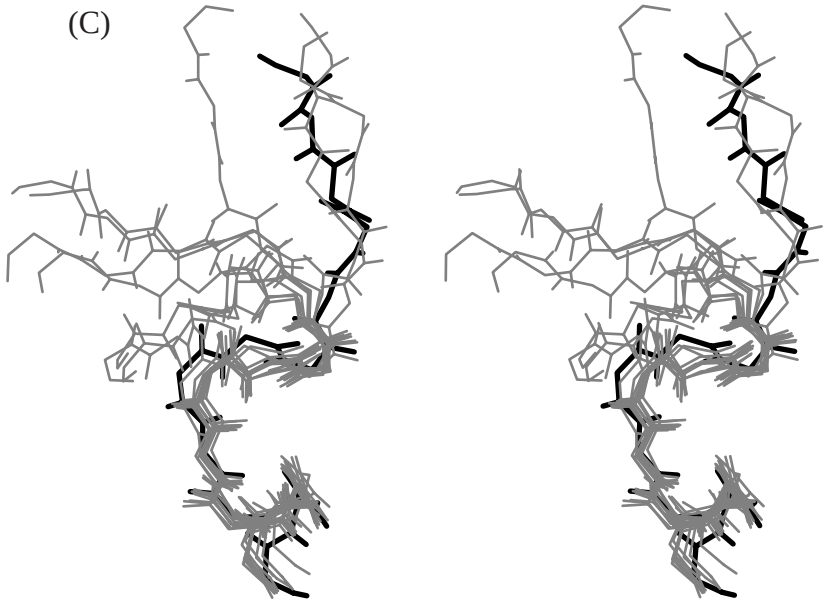

Figure 2. (continued).

distinguish effects on structural accuracy due to errors in the interproton distance estimates from the success of the rMD approach to generate the correct conformation. All of the NMR structures were subjected to a final optimization by energy minimization against the same empirical-energy potential function, E_{emp}, to obtain a meaningful comparison of geometry and nonbonded contacts. E_{emp} is the CHARMM22 force field including electrostatics and physically reasonable molecular mechanics parameters (MacKerell et al., 1998). Table 2 lists the information available following NMR structure determination and commonly used to assess the results: the empirical energy, NOE energy, and number of violations exceeding 0.1 Å and 0.2 Å. The values are averaged over 10 structures selected from the 100 generated by rMD, and the overall averages for the five approaches are also listed.

The NMR structures generated by rMD agree well with the NOE distances. For the helical peptide PKI(5–17), $\langle E_{\rm noe}^{smw} \rangle$ from 141 restraints is less than 5 kcal/mol, or 0.4 kcal/residue/mol, and the average number of violations above 0.2 Å is less than one per structure (Table 2). In the case of the coiled peptide, PKI(9–21), the distance restraints are less well satisfied by rMD; the $\langle E_{\rm noe}^{smw} \rangle$ values are somewhat larger ($\sim$0.6 kcal/residue/mol), and the average number of violations is 2.5 per structure. Similarly, when using the EXACT restraints, the helical peptide structures satisfy the restraints better than the structures determined for the coiled peptide. For both PKI(5–17) and PKI(9–21), the EXACT restraints produce structures with fewer violations and lower E_{noe} values than those obtained using the SMW restraints. Thus, accurate distance restraints appear to be more easily satisfied. That E_{noe} and E_{emp} in Table 2 are larger for the X-ray structure than for the NMR structures is in part due to the errors in the NMR restraints.

Particular to structures determined from etNOE is that the initial rMD simulations are done on the isolated peptide and the interactions with the protein are absent. Indeed, if the reference peptide is extracted from the complex and subjected to energy minimization, the NMR structures are found to match the resulting reference structure more closely; in the case of PKI(5–17), this process improves the accuracy of the NMR structures (defined below) by approximately 0.5 Å. This result suggests that the etNOE peptide structure could be improved by docking the peptide on the protein surface to include the intermolecular interactions in the rMD calculations.

Accuracy of the NMR structures

The accuracy of an NMR structure is defined here by its rms coordinate deviation from the starting reference structure. Deviations are averaged over all heavy atoms (AH), the main-chain backbone atoms N, Cα, and C (MC), or selected main-chain atoms (MC_{sel}). For PKI(5–17) the selected main-chain atoms are the

Table 2. Average energies and NOE violations for the rMD techniques used with each peptide

PKI(5–17) using SMW restraints

Approach	$\langle E_{emp}\rangle$[a]	$\langle E_{noe}^{SMW}\rangle$[b]	E_{emp}^{avg} [c]	E_{noe}^{avg}[d]	⟨Violations⟩	
					>0.1 Å	>0.2 Å
X-ray[e]	−28.10	138.74			12	8
X-ray[f]		0.23				
C1	−63.33	4.53	−52.39	4.87	6.7	0.7
C2	−50.96	3.96	−48.82	3.68	5.2	0.6
C3	−50.48	4.12	−58.23	4.66	5.3	0.5
C4	−56.29	4.23	−85.99	4.29	5.4	0.5
X1	−51.18	0.19	−57.83	0.10	0.0	0.0
Average[g]	*−54.45*	*3.41*	*−60.65*	*3.52*	*4.52*	*0.46*

Using EXACT restraints

Approach	$\langle E_{emp}\rangle$	$\langle E_{noe}^{EXACT}\rangle$	E_{emp}^{avg}	E_{noe}^{avg}	⟨ Violations ⟩	
					>0.1 Å	>0.2 Å
X-ray	−28.10	0.00			0	0
C1	−51.91	1.35	−50.21	1.30	0.0	0.0
C2	−46.87	1.98	−51.69	1.39	0.7	0.3
C3	−50.80	1.33	−50.42	1.31	0.3	0.1
C4	−50.89	1.33	−50.41	1.31	0.0	0.0
X1	−48.31	1.72	−50.32	1.44	0.9	0.0
Average[g]	*−49.76*	*1.54*	*−50.61*	*1.35*	*0.38*	*0.08*

PKI(9–21) Using SMW restraints

Approach	$\langle E_{emp}\rangle$	$\langle E_{noe}^{SMW}\rangle$	E_{emp}^{avg}	E_{noe}^{avg}	⟨Violations⟩	
					>0.1 Å	>0.2 Å
X-ray[e]	−123.96	54.77			12	10
X-ray[f]		0.00				
C1	−233.81	8.71	−211.68	8.28	9.5	2.4
C2	−190.11	8.11	−202.91	8.43	8.7	2.4
C3	−195.96	5.86	−179.36	7.07	7.1	1.1
C4	−187.01	8.41	−176.33	8.89	8.6	2.5
X1	−177.91	0.73	−184.09	1.68	0.4	0.0
Average[g]	*−196.96*	*6.36*	*−190.87*	*6.87*	*6.86*	*1.68*

Using EXACT restraints

Approach	$\langle E_{emp}\rangle$	$\langle E_{noe}^{EXACT}\rangle$	E_{emp}^{avg}	E_{noe}^{avg}	⟨Violations⟩	
					>0.1 Å	>0.2 Å
X-ray	−123.96	0.00			0	0
C1	−205.90	8.30	−199.42	9.50	9.3	1.2
C2	−151.94	4.94	−142.31	5.57	4.0	0.7
C3	−172.69	4.89	−171.53	5.62	4.6	0.8
C4	−169.12	4.12	−165.50	4.80	4.4	0.0
X1	−151.99	9.38	−135.07	12.70	5.9	1.8
Average[g]	*−170.33*	*6.33*	*−162.77*	*7.64*	*5.64*	*0.90*

[a] Average empirical energy from each ensemble.
[b] Average NOE energy from each ensemble.
[c] Empirical energy from the minimized average structure.
[d] NOE energy from the minimized average structure.
[e] NOE energy calculated using simple averaging of degenerate protons.
[f] NOE energy calculated using r^{-6} averaging of degenerate protons.
[g] Average value from the five rMD approaches.

helical residues Thr 5 to Ser 13, and for PKI(9–21) the selected main-chain atoms are those residues with medium-range or long-range NOE interactions, Asp 9 to Gly 17. Rms deviations are listed under the heading Accuracy in Table 3 as the average for the 10 NMR structures, and the single value for the average NMR structure after energy minimization.

The five approaches were found to give similar results, with no one approach consistently resulting in a set of more accurate structures. X1 generated a more accurate set of structures for PKI(5–17), but not for PKI(9–21). The results are therefore discussed hereafter in terms of the averages over all approaches. All figures are shown with structures from the C2 approach merely for consistency. Illustrations from the other four approaches are similar.

The global structure of the helical peptide PKI(5–17), with medium-range NOE interactions for nearly all residues, is well determined (Figure 2A); deviations from the target equal 0.8, 1.3 and 2.6 Å rms for MC_{sel}, MC, and AH, respectively (Table 3). Ramachandran plots of all individual residues (Laskowski et al., 1996) showed narrow distributions near the target value. Interestingly, although Thr 6 in the reference structure occupies a region of the Ramachandran plot that is energetically unfavorable, the NMR structure determination is able to reproduce this high-energy state of PKI(5–17). The ϕ, ψ distribution for Thr 6 from one of the NMR approaches (filled squares) is plotted in Figure 3A with the value for the reference structure (open square).

The overall main-chain conformation of the coiled peptide PKI(9–21), which lacks medium-range NOE interactions for residues 18 to 21, is determined (Figure 2B) but the accuracy is lower than that for PKI(5–17). The average rms deviation from the reference structure for PKI(9–21) is 1.0, 2.9 and 4.2 Å for MC_{sel}, MC, and AH, respectively (Table 3). The problem arises from the lack of medium and long-range NOE interactions for the C-terminal residues 18 to 21. A marked increase in conformational heterogeneity occurs at Gly 17, as seen in the distribution of the NMR structures viewed in Figure 2C after overlaying residues 9 to 17. Examination of the Ramachandran plot for Gly 17 (Figure 3B) finds a broad distribution, including values in high-energy regions. Such a broad distribution is not found for all glycine residues; Gly 14 in this peptide has a tight ϕ, ψ distribution, similar to the distribution for other residues in the peptide both preceding and following Gly 17. Thus, the structure of the selected residues 9 to 17, with mid-

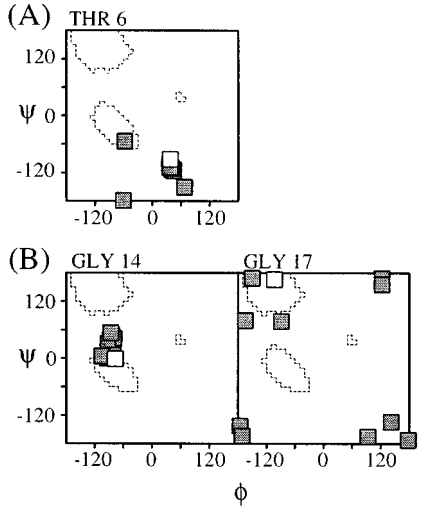

Figure 3. Selected individual Ramachandran plots for (A) PKI(5–17) residue Thr 6 and (B) PKI(9–21) residues Gly 14 and Gly 17, produced with approach C2 using the SMW restraint list. Angles from the reference structure are shown as open squares, results from the simulations are shown as filled squares.

range NOE interactions, is well determined. Yet the uncertainty of residues 17 to 20, which only have intraresidue and sequential NOE interactions, limits the global accuracy.

As a control, rMD was run without NMR restraints. The isolated, flexible peptide displays considerable conformational mobility, and the differences between the PKI structures and the reference structure are substantially larger (Table 4) than that after restrained molecular dynamics (Table 3). Thus, the et-NOE distance restraints effectively guide the molecular dynamics sampling toward the reference structure, and restrict the allowed conformational space to the appropriate region.

The accuracy of structures obtained with the upper bound of the E_{noe} restraint potential set to the exact distance in the reference structure (EXACT restraints) was determined to distinguish the effect of errors in the NMR distance restraints from the errors inherent in the rMD conformational search procedure itself. In the case of the helical peptide PKI(5–17), errors in the restraints did limit the structural accuracy. The MC and AH rms deviations between the reference structure and the NMR structures are reduced from 1.3 Å to 0.6 Å, and from 2.6 Å to 1.2 Å, respectively (Table 3). On the other hand, removing the error in the distance restraints for the extended peptide PKI(9–21) does not improve the global structural accuracy (MC rms difference is 2.8 Å for both SMW and EXACT re-

Table 3. Accuracy and precision of each rMD technique

PKI(5–17)	Accuracy						Precision		
Using SMW restraints	Ensemble average			Minim. avg. structure					
Approach	AH[c]	MC[d]	MC_{sel}[e]	AH	MC	MC_{sel}	AH	MC	MC_{sel}
C1	2.6	1.3	0.74	2.5	0.86	0.36	1.1	0.75	0.60
C2	3.0	1.5	0.89	3.0	1.5	0.84	0.67	0.35	0.35
C3	2.8	1.3	0.73	2.8	1.3	0.69	0.70	0.39	0.34
C4	3.1	1.6	1.1	2.9	1.5	1.0	0.92	0.64	0.64
X1	1.6	0.83	0.35	1.5	0.68	0.29	1.6	0.69	0.20
Average	*2.6*	*1.3*	*0.76*	*2.5*	*1.2*	*0.64*	*1.0*	*0.56*	*0.43*
Using EXACT restraints	Ensemble average			Minim. avg. structure					
Approach	AH	MC	MC_{sel}[f]	AH	MC	MC_{sel}	AH	MC	MC_{sel}
C1	1.2	0.57	0.22	1.0	0.58	0.22	0.48	0.15	0.01
C2	1.2	0.58	0.21	1.0	0.59	0.22	0.69	0.18	0.07
C3	1.1	0.59	0.23	0.92	0.58	0.23	0.48	0.12	0.02
C4	1.1	0.57	0.23	0.93	0.57	0.23	0.41	0.08	0.01
X1	1.3	0.56	0.20	1.1	0.50	0.21	1.1	0.40	0.10
Average	*1.2*	*0.57*	*0.22*	*0.99*	*0.56*	*0.22*	*0.64*	*0.19*	*0.04*

PKI(9–21)									
Using SMW restraints	Ensemble average			Minim. avg. structure					
Approach	AH	MC	MC_{sel}[f]	AH	MC	MC_{sel}	AH	MC	MC_{sel}
C1	4.1	2.3	1.0	3.6	1.9	0.83	2.9	2.0	0.42
C2	4.3	2.8	1.0	3.6	2.5	0.93	2.5	1.7	0.45
C3	4.9	3.7	1.1	3.8	3.2	1.2	3.0	2.0	0.36
C4	3.7	2.5	1.0	3.3	2.5	0.89	1.5	1.0	0.30
X1	4.2	2.9	0.88	3.3	2.6	0.95	4.7	3.3	0.84
Average	*4.2*	*2.9*	*1.0*	*3.5*	*2.5*	*0.97*	*2.9*	*2.0*	*0.47*
Using EXACT restraints	Ensemble average			Minim. avg. structure					
Approach	AH	MC	MC_{sel}	AH	MC	MC_{sel}	AH	MC	MC_{sel}
C1	4.6	3.0	0.78	4.3	2.1	0.92	3.4	2.5	0.52
C2	3.4	2.4	0.55	3.1	2.4	0.47	2.0	1.2	0.25
C3	3.2	2.0	0.50	3.3	1.8	0.45	2.0	1.2	0.18
C4	3.1	2.3	0.60	2.9	2.1	0.59	2.1	1.3	0.35
X1	3.9	2.5	0.58	4.2	2.1	0.57	4.0	2.7	0.48
Average	*3.6*	*2.4*	*0.60*	*3.6*	*2.1*	*0.60*	*2.7*	*1.8*	*0.36*

[a]Measured as an rms difference between the ensemble of best 10 structures and the X-ray structure.
[b]Measured as the average rms difference within the ensemble.
[c]All heavy (non-hydrogen) atoms.
[d]Main-chain N, Cα, C atoms.
[e]Main-chain atoms for residues 5–13.
[f]Main-chain atoms for residues 9–17.

Table 4. Accuracy and precision of the ensembles with no restraints for both model peptides

Approach and peptide model	Accuracy			Precision		
	AH	MC	MC_{sel}	AH	MC	MC_{sel}
UNRSTR PKI(5–17)	5.43	3.55	3.19	3.59	2.68	2.31
UNRSTR PKI(9–21)	6.42	4.00	2.91	4.04	2.96	2.45

straints), but does improve the results for residues 9 to 17, which participate in medium-range NOE interactions (MC_{sel} rms difference is 0.6 Å for EXACT and 1.0 Å for SMW restraints). The average NMR structure displays similar behavior (Table 3). The change in the NMR solutions when using EXACT restraints is visually illustrated by comparing the structures in Figure 4 with those in Figure 2. The improvements are clearly evident in panels A and C, while little change is apparent in panel B. These results show that more accurate restraints improve the structure except when the structure problem is poorly determined by the lack of enough structurally significant NOE interactions.

Precision of the NMR structures

The precision is defined as the average of the pairwise rms deviation between each of the 10 selected structures and the average NMR structure. Values are given in the last three columns of Table 3 for averages over the groups AH, MC and MC_{sel}. Coordinate differences are obtained following a least-squares superposition of atoms in the different groups. The precision of the structure determination is high in all comparisons of PKI(5–17) and for MC_{sel} from PKI(9–21). Most rms deviations are less than 1.0 Å and this convergence is visualized in Figures 2 and 4. That is, the NMR structures are more precisely determined than they are accurate, as found by previous simulation studies of NMR structure-determination methods (Clore et al., 1993; Zhao and Jardetzky, 1994).

Local precision and accuracy

An issue in the development of NMR methods for structure determination has been the question of whether precision of the NMR models is a useful indicator for the accuracy of the structural result. Consistent with earlier studies (Zhao and Jardetzky, 1994; Hoogstraten and Markley, 1996), precision of the whole molecule was not found to be a sensitive indicator for which of the rMD approaches generated the more accurate NMR structures. Values of E_{noe} and E_{emp} are also available to the experimentalist and could be used to judge the structure quality. While a number of structural models satisfied the restraints equally well and had favorable energy values, no correlation was found between accuracy and low energy. Thus, E_{noe} in the cases examined here is most useful for screening bad structural models, but is not a sensitive indicator of accuracy among models with low energy values.

Although there is no physical relationship that requires precision to be related to accuracy, circumstances may exist where precision is found to be a useful indicator. Clearly, the results in Table 3 show that both the accuracy and precision are higher for PKI(5–17) compared to PKI(9–21). Furthermore, both the accuracy and the precision improve when the distance restraints are changed from SMW to EXACT. In an attempt to obtain an estimate for the reliability of a structural model, we looked for some measure that might reflect the basis for this correspondence. The presence of mid-range NOE interactions was shown above to correlate with accuracy, which suggests that a local measure may be appropriate.

A local precision and accuracy were calculated using a three-residue average; atoms from a central residue and each neighboring residue are included in the least-square superposition of structures and in the rms summation. A representative plot shown in Figure 5 of the results generated with the SMW restraints demonstrates a correlation between the local precision and accuracy. The peaks in Figure 5C are Gly 17 of PKI(9–21), matching the imprecision of this residue with its inaccuracy. A similar degree of correlation is seen in the other four approaches.

Conclusions

Macromolecular systems of recognized and defined biological importance are increasingly more complex in character. Exchange-transferred NOE spectroscopy

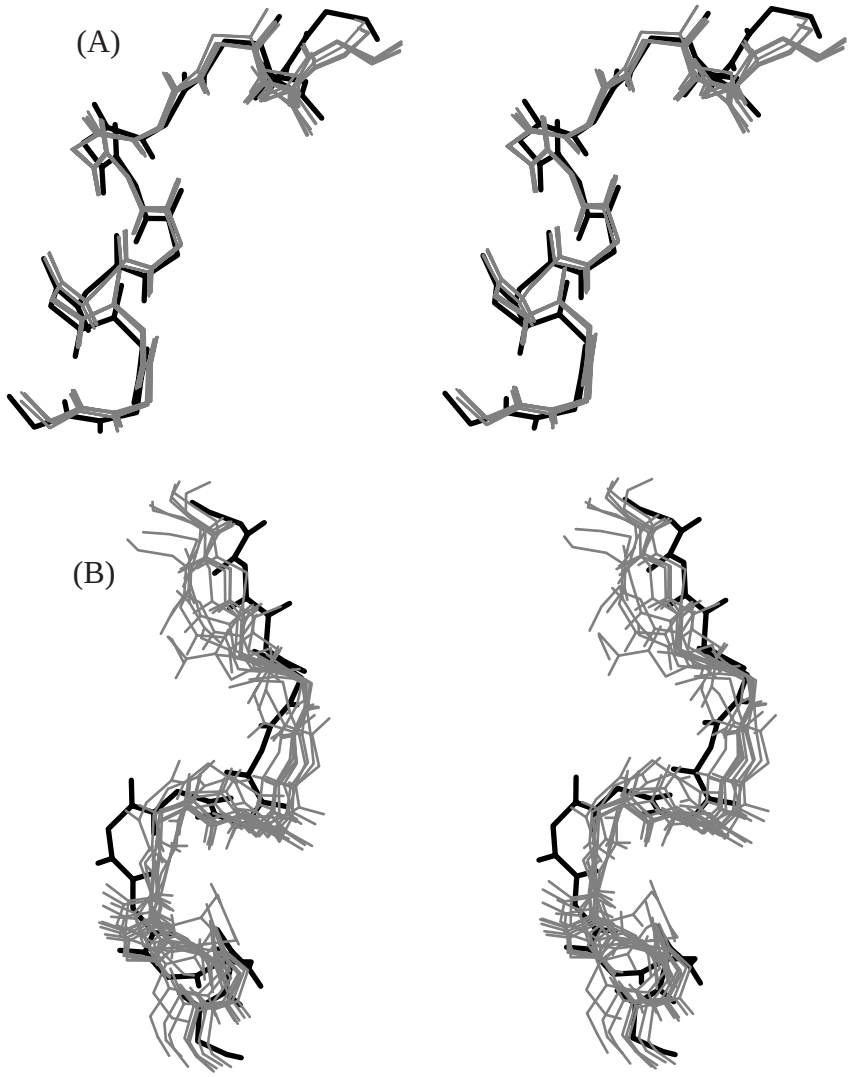

Figure 4. (A) Stereoview of a main-chain superposition of the best 10 structures of PKI(5–17) from the C2 EXACT restraints. The reference structure for this segment of PKI is shown in bold. (B) Same as (A) but with PKI(9–21). (C) Same as (B) but with a superposition of MC_{sel}, main-chain atoms for residues 9–17.

can play an important role for obtaining information about three-dimensional structural specificity and recognition for large protein complexes which are not amenable to study by X-ray crystallography. An important application of the etNOE method of structural analysis is to peptide–protein complexes which either involve inhibitory peptides or model protein–protein interactions. Distinctions between etNOE and direct NOE structure determination are the lower density of NOE contacts, the relaxation effects associated with the exchange process, and reduced packing interactions, including loose ends, typical of bound peptides. The results reported here examine the reliability of the structure of bound peptides determined from interproton distances estimated from etNOESY intensities in combination with restrained molecular dynamics.

The accuracy of the structures obtained from the etNOESY method was approximately 0.7 to 1.3 Å MC rms difference between the NMR structures and the reference structure when etNOE interactions were present between non-sequential residues. For regions where the interactions were limited to intraresidue and sequential contacts, the overall accuracy was reduced to approximately 2.5 to 3 Å rms difference from the reference structure. This level of accuracy results in a good model of the bound peptide, as evident visually

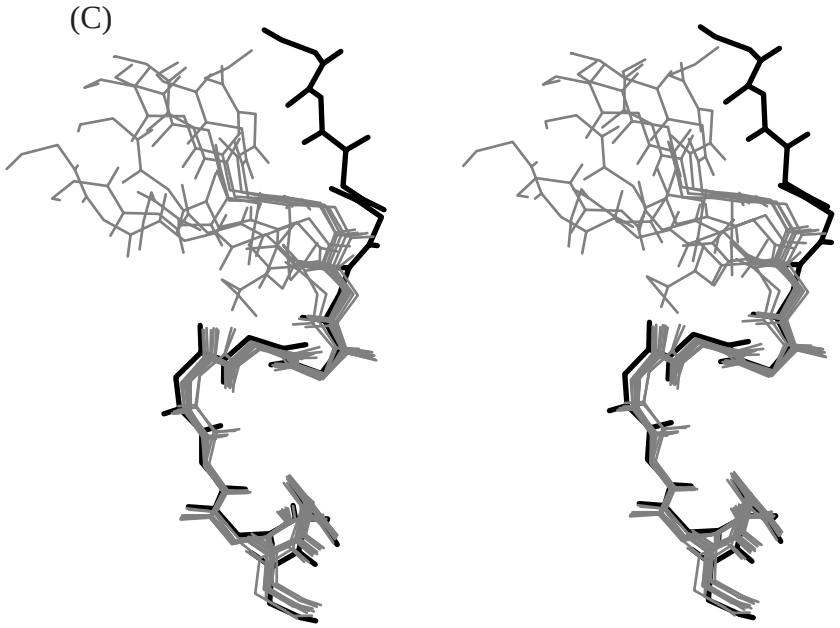

Figure 4. (continued).

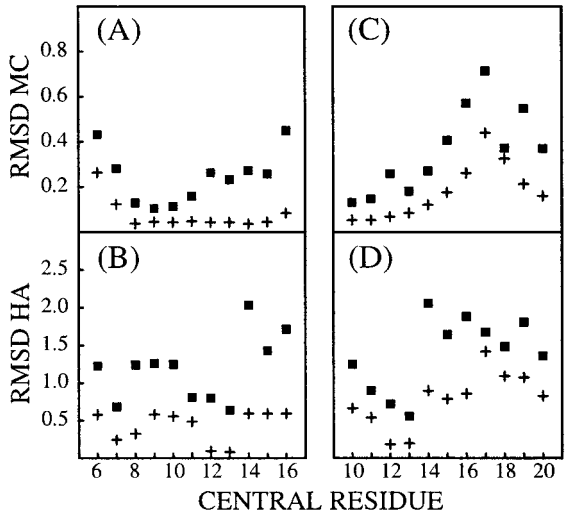

Figure 5. Local accuracy (filled squares) and precision (pluses) for main-chain (A) and all heavy (B) atom selections of PKI(5–17) and main-chain (C) and all heavy (D) atom selections of PKI(9–21) for approach C2. Local accuracy and precision were measured by overlaying three-residue increments from the ensembles with the SMW restraint list using the appropriate atom selection and measuring the rms difference along that same increment.

in Figure 2, but is somewhat lower than that reported for whole proteins (Clore et al., 1993; Zhao and Jardetzky, 1994; Hoogstraten and Markley, 1996). A variety of rMD approaches, differing by the presence or absence of electrostatic interactions or the inclusion of a fourth spatial dimension, were equally effective at generating reliable structures that satisfy the NMR restraints.

A critical factor for defining a reliable three-dimensional structure of the peptide is the occurrence of etNOE interactions between non-sequential residues. The results presented here demonstrate that a structure obtained for a peptide with a stretch of residues having only intraresidue and sequential etNOE interactions is less reliable. The total number of distance restraints per residue was approximately equal for the two peptides examined (∼11), yet the quality of the structural models varied. Thus, the pattern of NOE interaction, rather than the total number of distance restraints per residue, is important. This point can be appreciated by considering, for example, that one or two mid-range NOE interactions could reasonably define the main-chain conformation of a four-residue tight turn. The presence of non-sequential NOE interactions over most of the peptide is particularly important for etNOE structure determination since packing effects are absent and the ends are not tied down as would be the case for surface loops in a protein. When a stretch of residues lacks mid- or long-range NOE interactions, a number of conformations were found that satisfied the intraresidue and sequential restraints but differed in their overall global structure. Docking the peptide onto the protein surface

may be a reasonable approach in this case for selecting the correct peptide structure from the set of structures obtained for the isolated peptide.

It is of interest to note that most of the distance violations greater than 0.2 Å in the peptide structures correspond to incorrectly categorized distances. The errors in these restraints were due to degenerate NOE pairs, such as Y10 $H_{\delta1,\delta2}$–Y10 H_{α} and Y7 $H_{\delta1,\delta2}$–F10 $H_{\delta1,\delta2}$, and vicinal protons of methylene groups, that required distance averaging for the restraint target. Increased upper bounds for distances estimated from a degenerate cross peak (Eisenmesser and Post, 1998; Maurer et al., 1999) could improve the structural accuracy.

Intermolecular spin diffusion through the protein does not give rise to errors in distance restraints. The lack of any significant influence from protein protons on the ligand etNOE intensities shown in Figure 1 for an actual protein–peptide complex is consistent with results from a three-spin simulation study (Zheng and Post, 1993) in light of the absence of protein protons proximal to peptide protons. Indirect spin-diffusion effects from protein protons were shown to be insignificant unless the distance from the protein proton to both ligand protons is shorter than the distance between the two ligand protons. Simulations of protein–peptide complexes other than PKI•PKA also show negligible effects from the protein (Zabell and Post, unpublished results). Together, these results indicate that it is rare to have a protein proton positioned at a short enough distance between two peptide protons to give rise to a strong indirect effect, and that spin-diffusion through the protein is not a likely problem for structure determination of the peptide by using the etNOE approach.

Previous studies which examined the NMR structure determination of whole proteins (Clore et al., 1993; Zhao and Jardetzky, 1994; Bassolino-Klimas et al., 1996; Hoogstraten and Markley, 1996) considered a means by which an accurate structure, or set of structures, can be distinguished from a poorly determined structural solution. One possibility is a correlation between precision and accuracy. As carefully discussed (Zhao and Jardetzky, 1994), no correlation need exist. Nonetheless, it is useful to examine the possibility that such a correlation does exist since precision is the only parameter available to the experimentalist. In agreement with the aforementioned work, we find no correlation between global accuracy and precision when comparing results obtained by the five different rMD approaches (e.g. C3 versus X1), but a relationship was found between the precision and accuracy defined on a local scale of three-residue segments. This relationship is not caused by structural bias in the reference structure of this simulation study, since the reference structure is from crystallographic coordinates that do not optimally fit the rMD target potential function. The correlation is reasonable given the strong dependence of accuracy on the existence of etNOE interactions between non-sequential residues. In the case of peptides, these interactions are predominantly restraint pairs separated by two or three intervening residues. The local precision is reflecting the impact of these structurally valuable restraints. The dependence of accuracy on the number of mid- and long-range NOE interactions, rather than the total number of restraints, is probably not limited to peptide ligand structure. The improved accuracy of whole protein structures reported in the literature has coincided with an increase in the number of distance restraints, yet a longer list of restraints likely includes an increase in those restraints with long-range structure defining value.

Acknowledgements

This work was supported by a grant to C.B.P. from the NIH (R01-GM39478). C.B.P. was supported by a Research Career Development Award from the NIH (K04-GM00661) and A.P.R.Z. and E.Z.E. received a training fellowship from the NIH (5T32-GM08296). The NMR facility is supported by a grant to the Purdue Cancer Center. The computing facilities shared by the Structural Biology group were supported by grants from the Lucille P. Markey Foundation and the Purdue University Academic Reinvestment Program.

References

Albrand, J.P., Birdsall, B., Feeney, J., Roberts, G.C.K. and Burgen, A.S.V. (1979) *Int. J. Biol. Macromol.*, **1**, 37–41.

Andersen, N.H., Nguyen, K.T. and Eaton, H.L. (1985) *J. Magn. Reson.*, **63**, 365–375.

Andrieux, M., Leroy, E., Guittet, E., Ritco-Vonsovici, M., Mouratou, B., Minard, P., Desmadril, M. and Yon, J.M. (1995) *Biochemistry*, **34**, 842–846.

Arepalli, S.R., Glaudemans, C.P.J., Daves Jr., G.D., Kovac, P. and Bax, A. (1995) *J. Magn. Reson.*, **B106**, 195–198.

Ashby, C.D. and Walsh, D.A. (1972) *J. Biol. Chem.*, **247**, 6637–6642.

Barsukov, I.L., Lian, L.Y., Ellis, J., Sze, K.H., Shaw, W.V. and Roberts, G.C.K. (1996) *J. Mol. Biol.*, **262**, 543–558.

Bassolino-Klimas, D., Tejero, R., Krystek, S.R., Metzler, W.J., Montelione, G.T. and Bruccoleri, R.E. (1996) *Protein Sci.*, **5**, 593–603.

Brooks, B.R., Bruccoleri, R.E., Olafson, B.D., States, D.J., Swaminathan, S. and Karplus, M. (1983) *J. Comput. Chem.*, **4**, 187–217.

Brünger, A.T. (1992) *X-PLOR 3.1: A System for X-ray Crystallography and NMR*, Yale University Press, New Haven, CT.

Burritt, J.B., Busse, S.C., Gizachew, D., Siemsen, D.W., Quinn, M.T., Bond, C.W., Dratz, E.A. and Jesaitis, A.J. (1998) *J. Biol. Chem.*, **273**, 24847–24852.

Campbell, A.P. and Sykes, B.D. (1991) *J. Magn. Reson.*, **93**, 77–92.

Campbell, A.P. and Sykes, B.D. (1993) *Annu. Rev. Biophys. Biomol.*, **22**, 99–122.

Casset, F., Imberty, A., Perez, S., Etzler, M.E., Paulsen, H. and Peters, T. (1997) *Eur. J. Biochem.*, **244**, 242–250.

Clore, G.M., Brünger, A.T., Karplus, M. and Gronenborn, A.M. (1986) *J. Mol. Biol.*, **191**, 523–551.

Clore, G.M. and Gronenborn, A.M. (1983) *J. Magn. Reson.*, **53**, 423–442.

Clore, G.M., Nilges, M., Brünger, A.T., Karplus, M. and Gronenborn, A.M. (1987) *FEBS Lett.*, **213**, 269–277.

Clore, G.M., Robien, M.A. and Gronenborn, A.M. (1993) *J. Mol. Biol.*, **231**, 82–102.

Eisenmesser, E.Z. and Post, C.B. (1998) *Biochemistry*, **37**, 867–877.

Feeney, J., Birdsall, B., Roberts, G.C.K. and Burgen, A.S.V. (1983) *Biochemistry*, **22**, 628–633.

Fletcher, R. and Reeves, C.M. (1964) *Comput. J.*, **7**, 149–154.

Fraenkel, Y., Shalev, D.E., Gershoni, J.M. and Navon, G. (1996) *Crit. Rev. Biochem. Mol.*, **31**, 273–301.

Fraternali, F., Do, Q.-T., Doan, B.-T., Atkinson, R.A., Palmas, P., Sklenar, V., Safar, P., Wildgoose, P., Strop, P. and Saudek, V. (1998) *Proteins*, **30**, 264–274.

Gizachew, D., Moffett, D.B., Busse, S.C., Westler, W.M., Dratz, E.A. and Teintze, M. (1998) *Biochemistry*, **37**, 10616–10625.

Gunasekaran, K., Ramakrishnan, C. and Balaram, P. (1996) *J. Mol. Biol.*, **264**, 191–198.

Hoogstraten, C.G. and Markley, J.L. (1996) *J. Mol. Biol.*, **258**, 334–348.

Jackson, P.L., Moseley, H.N.B. and Krishna, N.R. (1995) *J. Magn. Reson.*, **B107**, 289–292.

Kleywegt, G.J. and Jones, T.A. (1996) *Structure*, **4**, 1395–1400.

Knighton, D.R., Zheng, J., Ten Eyck, L.F., Xuong, N.-H., Taylor, S.S. and Sowadski, J.M. (1991) *Science*, **253**, 414–420.

Kobayashi, N., Freund, S.M.V., Chatellier, J., Zahn, R. and Fersht, A.R. (1999) *J. Mol. Biol.*, **292**, 181–190.

Kraulis, P.J., Clore, G.M., Nilges, M., Jones, T.A., Pettersson, G., Knowles, J. and Gronenborn, A.M. (1989) *Biochemistry*, **28**, 7241–7257.

Laskowski, R.A., Rullmann, J.A.C., MacArthur, M.W., Kaptein, R. and Thornton, J.M. (1996) *J. Biomol. NMR*, **8**, 477–486.

Levy, H.R., Ejchart, A. and Levy, G.C. (1983) *Biochemistry*, **22**, 2792–2796.

London, R.E., Perlman, M.E. and Davis, D.G. (1992) *J. Magn. Reson.*, **97**, 79–98.

Machida, M., Yokoyama, S., Matsuzawa, H., Miyazawa, T. and Ohta, T. (1985) *J. Biol. Chem.*, **260**, 16143–16147.

MacKerell, A.D.J., Bashford, D., Bellott, M., Dunbrack, R.L., Evanseck, J.D., Field, M.J., Fischer, S., Gao, J., Guo, H., Ha, S., Joseph-McCarthy, D., Kuchnir, L., Kuczera, K., Lau, F.T.K., Mattos, C., Michnick, S., Ngo, T., Nguyen, D.T., Prodhom, B., Reiher, W.E., Roux, B., Schlenkrich, M., Smith, J.C., Stote, R., Straub, J. and Karplus, M. (1998) *J. Phys. Chem.*, **B102**, 3586–3616.

Matsunaga, T.O., Collins, N., Ramaswami, V., Yamamura, S.H., O'Brien, D.F. and Hruby, V.J. (1993) *Biochemistry*, **32**, 13180–13189.

Maurer, M.C., Trosset, J.Y., Lester, C.C., DiBella, E.E. and Scheraga, H.A. (1999) *Proteins*, **34**, 29–48.

Mayo, K.H., Fan, F., Beavers, M.P., Eckardt, A., Keane, P., Hoekstra, W.J. and Andrade-Gordon, P. (1996) *Biochemistry*, **35**, 4434–4444.

Metzler, W.J., Hare, D.R. and Pardi, A. (1989) *Biochemistry*, **28**, 7045–7052.

Moseley, H.N.B., Curto, E.V. and Krishna, N.R. (1995) *J. Magn. Reson.*, **B108**, 243–261.

Ni, F. (1994) *Prog. NMR Spectrosc.*, **26**, 517–606.

Ni, F. and Scheraga, H.A. (1994) *Acc. Chem. Res.*, **27**, 257–264.

Ni, F. and Zhu, Y. (1994) *J. Magn. Reson.*, **B103**, 180–184.

Poppe, L., Brown, G.S., Philo, J.S., Nikrad, P.V. and Shah, B.H. (1997) *J. Am. Chem. Soc.*, **119**, 1727–1736.

Post, C.B. (1992) *J. Mol. Biol.*, **224**, 1087–1101.

Post, C.B., Meadows, R.P. and Gorenstein, D.G. (1990) *J. Am. Chem. Soc.*, **112**, 6796–6803.

Ramesh, V., Syed, S.E.H., Frederick, R.O., Sutcliffe, M.J., Barnes, M. and Roberts, G.C.K. (1996) *Eur. J. Biochem.*, **235**, 804–813.

Scherf, T., Hiller, R., Naider, F., Levitt, M. and Anglister, J. (1992) *Biochemistry*, **31**, 6884–6897.

Schneider, M.L. and Post, C.B. (1995) *Biochemistry*, **34**, 16574–16584.

Sokolowski, T., Haselhorst, T., Scheffler, K., Weisemann, R., Kosma, P., Brade, H., Brade, L. and Peters, T. (1998) *J. Biomol. NMR*, **12**, 123–133.

van Schaik, R.C., Berendsen, H.J.C., Torda, A.E. and van Gunsteren, W.F. (1993) *J. Mol. Biol.*, **234**, 751–762.

Verlet, L. (1967) *Phys. Rev.*, **159**, 98–105.

Vincent, S.J.F., Zwahlen, C., Post, C.B., Burgner II, J.W. and Bodenhausen, G. (1997) *Proc. Natl. Acad. Sci. USA*, **94**, 4383–4388.

Walsh, D.A., Ashby, C.D., Gonzalez, C., Calkins, D., Fischer, E.H. and Krebs, E.G. (1971) *J. Biol. Chem.*, **246**, 1977–1985.

Zhao, D. and Jardetzky, O. (1994) *J. Mol. Biol.*, **239**, 601–607.

Zheng, J. and Post, C.B. (1993) *J. Magn. Reson.* **B101**, 262–270.

Zheng, J. and Post, C.B. (1996) *J. Phys. Chem.*, **100**, 2675–2680.